AEROACOUSTIC VALIDATION OF THE FREE WAKE METHOD FIRST ON THE BASIS OF A H145 MAIN ROTOR IN DESCENT FLIGHT

Patrick P. Kranzinger, Manuel Keßler, and Ewald Krämer

Institute of Aerodynamics and Gas Dynamics (IAG), University of Stuttgart
Pfaffenwaldring 21, 70569 Stuttgart, Germany
kranzinger@iag.uni-stuttgart.de

Abstract

To resolve aeroacoustic phenomena of helicopter rotors with CFD computations, very detailed, finely discretized, big and consequently expensive simulations setups are required. As the significance of the noise emission of helicopters is continuously increasing in terms of certification and regulation, a more efficient but also reliable and sufficiently accurate simulation method is mandatory. With today's computational power free wake methods fulfill all of these attributes, as they can predict the main drivers of aeroacoustic noise emissions of rotors for the most certification relevant flight states correctly. Within the recent years at IAG the free wake method FIRST has been developed at IAG, which can be weakly coupled to flight mechanic tools such as CAMRAD II and (G)HOST. By means of a BVI forward descent flight state, FIRST is validated comparing the aerodynamic and aeroacoustic results to CFD computations and acoustic flight test data.

1 NOTATION

BVI	blade vortex interaction
BPF	blade passing frequency
CAA	Computational Aero-Acoustics
CFD	Computational Fluid Dynamics
CSD	Computational Structure Dynamics
EPNL	Effective Perceived Noise Level
FW-H	Ffowcs Williams-Hawkings
GP	ground plate
MR	main rotor
PNLT	tone corrected Perceived Noise Level
R	rotor radius
r_c	vortex core radius
$\frac{r}{R}$	relative blade radial station
SPL	Sound Pressure Level
TAS	true air speed

2 INTRODUCTION

Society's noise sensitivity increased during the recent past while the mission profile of helicopters has been continuously extending. On this account, it is compulsory to consider a helicopter's noise emission already in early design phases.

Recent advances in the field of higher order methods and the increasing power of high performance computation clusters enabled very accurate prediction of the aero-acoustic footprint of helicopters by CFD solvers [1] [2]. However, enormous computational power is required to investigate even a single flight case, which is inadequate for general industrial purposes during the design phase of rotor systems. Especially during landing approaches in slow descent flight, helicopters show strong, unpleasant noise emission when rotor blades interact with the blade tip vortices of the preceding blade. In the past low fidelity free wake methods showed already qualitative agreement on resolving this aeroacoustic phenomenon called blade vortex interaction (BVI) [3].

Todays available computing power allows increasing spatial and temporal discretization of free wake simulations, by which their reliability, prediction quality and agreement with CFD results and experimental data is further improved. Considerably, this makes free wake methods a first choice when BVI noise estimation is required in conjunction with limited computing resourcesor for exploration of large design spaces.

In recent years, the free wake IAG Rotor Simulation Tool (FIRST) was developed by the Institute of Aerodynamics and Gas Dynamics, which allows fast examination of different rotor and complete helicopter configurations with regard to BVI noise. For validating the aeroacoustic capabilities of our CFD tool chain in combination with the newly developed free wake solver FIRST, a 6 ° slow forward descent BVI flight situation of the Airbus Helicopters' H145 main rotor is investigated and compared to recently published CFD-computations and experimental data.

3 METHODS

3.1 Free wake

FIRST is a stand-alone aerodynamics solver for multi-rotor systems based on the instationary potential theory: For stationary, three-dimensional and frictionless cases, e.g. for a stationary forward flight of fixed wing aircrafts, the wake can be modelled by a continuous chordwise vorticity distribution representing the spanwise gradient of the local lift, featuring two strong tip vortices. In instationary situations, e.g. for maneuver flight of fixed wing aircrafts or the forward flight of a helicopter, the upstream conditions for the wings respectively for the rotor blades are continuously changing. Thus, the local lift distribution underlies a temporal variation, which leads to changes of the vorticity distribution of the wake.

Contrary to some simple stationary cases, there is no analytical solution. Hence, the problem needs to be discretized and solved numerically. Therefore, FIRST uses a spatial discretization in spanwise direction of the wake. The vorticity layer is modelled by discrete linear vortex filaments, which edge points are freely moving in space due to the induction of all other elements. Within every time step the currently induced velocity at the endpoints of each filament is computed. The wake development is then achieved by integration using a explicit 5th order Predictor-Corrector scheme based on the Adams-Bashforth and Adams-Moulton method.

The disregard of friction would lead to physically unlikely high flow speeds close to discrete vortex filaments, for which reason vortex core models are used to stabilize the method and express the induced velocity correctly. FIRST is featuring the Rankine, Scully and Vatistas vortex model[4][5][6][7]. A further side effect neglegting of friction is the complete absense of dissipation. Thus, if no empiric dissipation model is applied, the vortex strength of each filament of the wake is being constant. FIRST supports vortex dissipation and aging models.

Due to the method complexity the best strategy to accelerate the solution beside the application of Fast Multi Pole methods, is to reduce the number of vortex filaments accounted. FIRST features vortex aggregation and dropping on the basis of their distance to defined areas of interest. This allows a variable reduction of the resolution with increasing distance to the components investigated, without losing absolute energy conserved within the flow field.

FIRST features lifting line, lifting surface and lifting body models as well as displacers (like a fuselage). Movements of different structure components, as e.g. blades and the fuselage, are represented by a freely configurable motion tree. FIRST is shared memory parallelized using POSIX threads on the intra-node level and uses MPI for inter-node communication.

Linking against IAG-developed libraries used for structure deformation and load evaluation[8][9] provides interfaces for automated weak and strong coupling to different computational structure dynamics (CSD) and flight mechanics tools (as e.g. CAMRAD II[10] or (G)HOST[11]). As FIRST is sharing the coupling interface libraries with FLOWer, the weak coupling tool chain used with FLOWer can be reused including the coupling controlling tool HeliCats[12].

3.2 Flight Mechanics (FM) and Structural Dynamics (CSD)

For helicopter applications, a proper reproduction of the flight state including the aero-elasticity of the rotor blades is mandatory. Especially in forward flight, blade elasticity influences the aerodynamic behavior and force generation substantially.

At IAG, the structural deformation of the rotor blades is modelled using the Comprehensive Analytical Model of Rotorcraft Aerodynamics and Dynamics (CAMRAD II) code as part of a weak coupling scheme: The CAMRAD II code provides solutions for the blade deformation and flight kinematics, modelling the rotor blades as Euler-Bernoulli beams with isotropic material and elastic axes. For aerodynamics load estimations a low-fidelity aerodynamics model based on lifting line theory and two dimensional steady airfoil data tables is used there. These initial deformation and trim-angle values are used for performing a CFD based aerodynamics simulation, providing load results of high-fidelity. Correcting the internal low-fidelity loads evaluation of CAMRAD II with the CFD results, the CSD internal aerodynamics are successively replaced by the CFD, respectively free wake based loads, leading to blade dynamics based on CFD/free wake loads with deformation and deflection calculated with CSD.

In order to fit the specified global forces and moments, in case of an isolated rotor trim the collective and two cyclic control angles are determined with a fixed rotor orientation, known as the wind-tunnel trim. For a complete helicopter, three additional degrees of freedom are taken into account for the spatial fuselage orientation and the tail rotor thrust. This approach is designated as a free-flight trim.

3.3 Aeroacoustics (CAA)

For computing the aeroacoustic nose emission, the IAG developed CAA code ACCO[13] is used.

As basis for the computation serves the absolute load distribution along the quarter chord of every rotor blade over time. Therefore, the resulting pressure fluctuations at the surface of the rotor blades are reduced to local force vectors by sectional integration within every time step.

Acoustic modelling is achieved by using the Ffowcs-Williams-Hawkings (FW-H) equation

$$(1) \qquad \frac{\overline{\partial}^2 \overline{\rho}'}{\partial t^2} - c^2 \overline{\nabla}^2 \rho' = \frac{\partial}{\partial x_i}[p' n_i \delta(f)] + \frac{\partial}{\partial t}[\rho_0 v_n \delta(f)]$$

where $\overline{\rho}'$ is the time averaged density fluctuation, p the pressure fluctuation, n_i the normal vector, v_n the normal component of the surface velocity, and $\delta(f)$ the Dirac delta function.

With the use of the wave equation on the left hand side and Lighthill's analogy, undisturbed freestream conditions are assumed for the complete volume. The right hand side of the equation represents the source terms. As FIRST is a potential flow solver, only load fluctuations (dipoles) can be directly provided. Noise emissions resulting from volume displacement are directly computed within ACCO using a threedimensional surface mesh of the rotor blades and corresponding movement information.

As free wake methods are based on potential theory, no qadrupole source terms mainly resulting from shear layer influences or turbulence and compression shocks can be taken into account. Usually, for helicopter rotor simulations, only a small part of the resulting aeroacoustic emission is alloted to quadrupole terms. In the considered BVI flight state, the main noise emission can be traced back to load fluctuations on the surface of the rotor blades.

Having the FW-H equation solved, time domain acoustic pressure can be calculated at arbitrary locations in space, called observers. Finally, the specific aeroaoustic values such as narrow-band spectra, Sound Pressure Level (SPL) and Perceived Noise Level (PNL) are derived from the acoustic pressure information.

4 VALIDATION TEST CASE

Free wake methods allow good prediction of the position of the tip vortices and their strength within the rotor disk area in terms of the required computation power in relation to the quality of the results. The prediction of aeroacoustic emissions for BVI flight states is one of the most critical scopes of application concerning its accuracy, as slight misplacements of the tip vortices have strong influence on the aeroacoustic results.

Consequently, to assess the acoustic predictive capabilities of the new FIRST based free wake process

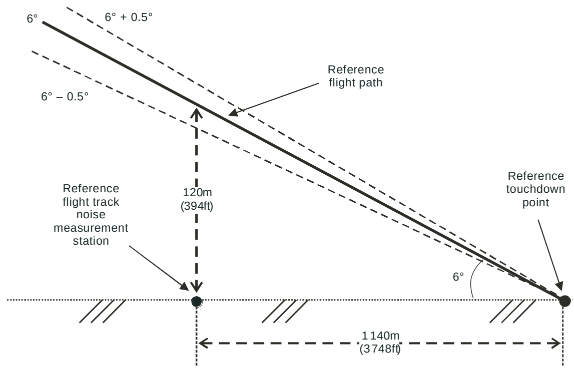

Figure 1. Schematic overview to the flight boundaries of the approach test conditions[14].

chain, a certification relevant slow forward, descent flight state is chosen as validation test case. As specified within the helicopter noise certification rules and regulations[14], three microphones are placed in a line perpendicular to the flight path at the ground with a distance of 150 m to each other. As schematically illustrated in Figure 1, the helicopter follows its 6 ° descent flight path orthogonally to the microphone array with a flight speed correlating to the speed at its best rate of climb. Thereby, the center microphone is overflown at an altitude of 120 m.

Differing to the noise certification procedure the experimental data is recorded using microphones which were placed above ground plates (cf. Figure 2). So the signal experiences a defined total reflection on the ground plate (GP), contrary to simulation results. This can be considered during evaluation of the pressure time signals derived from the simulations by their doubling. Aeroacoustic key values are computed according to the ICAO evaluation procedure. For the evaluation, the microphones signals are considered as measured in form of pressure-time signals.

The aerodynamic and aeroacoustic results are compared to CFD results published by Kowarsch et. al 2015[1] and to experimental flight test data recorded during the noise measurement campaign of the H145 in 2012[15]. Table 1 summarizes the main attributes of

Attribute	
Rotor blades	4
Rotor radius	5.5 m
Rotor rpm	96.6 %
TAS	70 kn
Flight path angle	6.0 °
Hight over microphones	120 m
No. of microphones	3
EPNL (ICAO)	90.3 EPNdB

Table 1. Main attributes of the H145 MR geometrie and of the flight test conditions and results.

the H145 main rotor as well as the averaged testing conditions. For the further numerical investigations the wind speed data is not considered.

5 TRIMMING

For validation purposes, only the main rotor of the H145 is considered. To get an accurate trimmed flight state as reference for the aeroacoustic validation computations, a setup is chosen which corresponds to a good compromise concerning temporal and spatial accuracy and computational costs. Based on experience, the rotorblades are modelled as lifting surfaces with five equidistant distributed chordwise panels and 25 spanwise panels distributed using sinusoidal distribution function. The temporal discretization is chosen at 2 °.

As shown in Figure 2, the induced velocity profiles of the different available vortex core models only differ for radii $\frac{r}{r_c} < 2$. Young has shown that the physical vortex core size r_c behind a helicopter rotor blade lies between 10^{-2} and $10^{-3}R$[16]. To get spanwise resolution representing a continous vortex layer trailing the helicopter rotor blades, the distance between vortex trailers needs to be of a size of the vortex core radius which correlates to 100-1000 spanwise trailers. If less trailers are used, either the core size needs to be increased to non-physical values or the velocity field behind the rotor blade is not smooth anymore. Due to the method complexity, increasing the number of trailers has a significant influence on the computation time required for running the simulation. However, experience shows, that even with 15 trailers or less and vortex core sizes greater than 150 mm good aeroacoustic agreement can be achieved[3].

Consequently, for all productive computations the number of trailers is chosen much smaller than required for modelling vortex cores based on a physically correct resolution. On this account, the detailed modelling of the viscous vortex plays a minor role in terms of the aerodynamic and aeroacoustic results. For all computations within this study, the Rankine vortex model is selected, because of its numerical simplicity (and consequently speed). To show the stability of the free wake implementation a vortex core radius of only 25 mm is chosen. As for usual forward flight states dissipation becomes only significant, when the wake has left the influence area of the rotor, disregarding of dissipation has no noticeable influence to the solution, which is why vortex dissipation and aging have been disabled to reduce the number of empiric parameters within the validation process.

The goal of the trim setup is to get a validated reference solution which features as few as possible empirical parameteres. Therefore the application of acceleration methods as vortex filament aggregation and dropping is renounced. All vortex filaments are

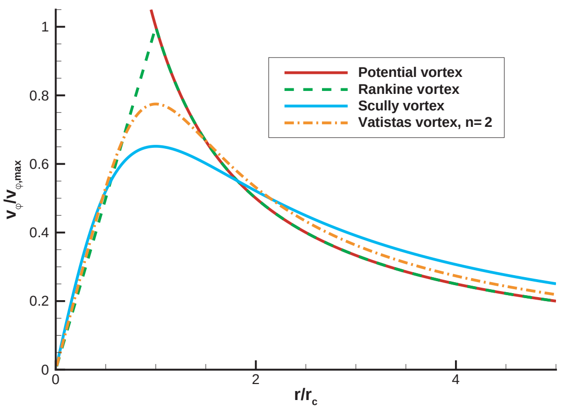

Figure 2. Comparison of the induced tangential velocity of different vortex core models.

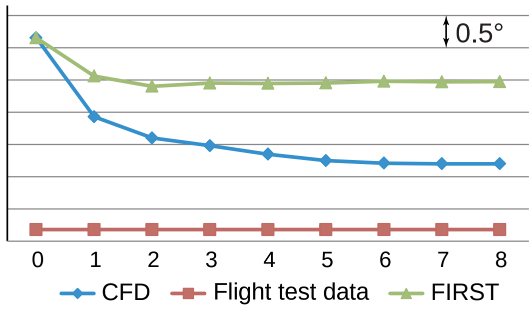

(a) Collective pitch

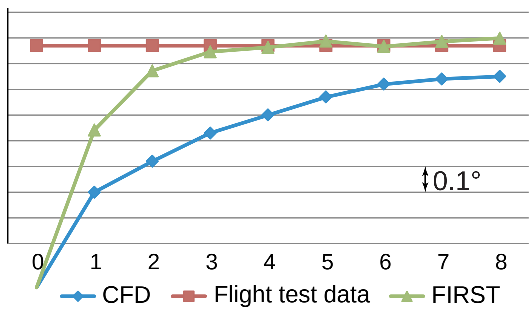

(b) Lateral cyclic pitch

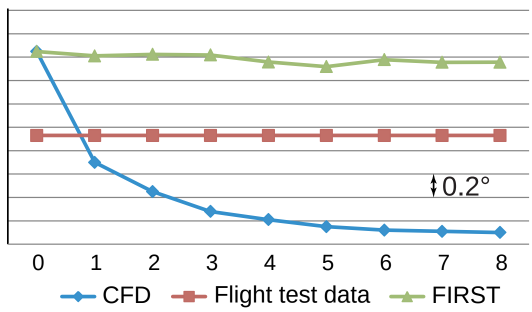

(c) Longitudinal cyclic pitch

Figure 3. Development of the trim angles by trim iterations. **CFD reference values by Kowarsch et al.[1]**

dropped after they left the influence area of the rotor disk after two complete rotor revolutions.

For validating FIRST, the isolated rotor configuration is weakly coupled to CAMRAD II using the wind tunnel trim scheme. HeliCats is used to control the complete trim process. For computing the structure dynamics the same model as used for the reference CFD computations by Kowarsch et al.[1] is applied. As the used lifting surface model allows only a very rough evaluation of local pitching moments, only the sectional forces are used for correcting the internal blade element aerodynamics of CAMRAD II. When correcting only parts of the aerodynamic loads within a weak coupling scheme, the not-corrected parameters are updated with the values provided by the internal aerodynamics model of the flight mechanic tool. Practically, this means when only correcting the forces, CAMRAD II uses the polar values for the pitching moments, which corresponds to the corrected aerodynamic forces provided by the free wake model.

The first retrim is executed after 720 time steps, what corresponds to four rotor revolutions, to ensure a complete convergence of the solution. All following retrims are executed after 360 subsequent time steps. For the trim computations FIRST is run on a single node of the Hazel Hen computation cluster of the HLRS at Stuttgart. Parallelization is achieved using shared memory in combination with 24 POSIX threads. As with this configuration a 360 ° trim run takes only 18 min, which is less than the CAMRAD II execution for retrimming, no further parallelization is required. Experimentally, the parallelization was extended to use two nodes with 24 threads each, what reduced the required wall clock time to 10 min.

As shown in Figure 3, convergence is achieved after eight trim runs respectively four hours of total wall clock time. The number of retrims required is comparable to the experiences made by coupling the CFD code FLOWer weakly to the same configuration. Due to the chosen setup with 26 trailers per blade with an average distance of ca. 180 mm in combination with a vortex core radius of 25 mm, no smooth induced velocity field within the wake results. Although the global aerodynamic characteristics of the flow field are reflected correctly, the solution will never converge completely from a numerical point of view. Because of the spatial underdiscretization the exact positions of the vortex filaments within the main aerodynamic structures are subject to stochastic effects. This problem can be overcome by increasing the vortex core size to values greater than the average spanwise trailer distance at the expense of non-physical assumptions for the viscosity within the vortex cores. To show that in spite of the underdiscretization no divergence will occur, the trim procedure is continued until 25 trim iterations are completed. Thereby, the method showed excellent robustness. The uncertainties in the solution let all trim angles stochastically vary within a bandwith of less than 0.08 °, which is below the accuracy that can be achieved within flight tests.

In comparison with CFD and experimental data, the resulting trim angles show very good agreement. Lateral and longitudinal pitch fit the experimental data even better, than the CFD solution. The offset of the collective can be explained by the very rough aerodynamic model of the rotor blade and the disregard of the pitching moments for the trim. Hence, for further, more detailed investigations, the usage of a more accurate lifting body model is advisable, which allows to take the local pitching moments into account for trimming.

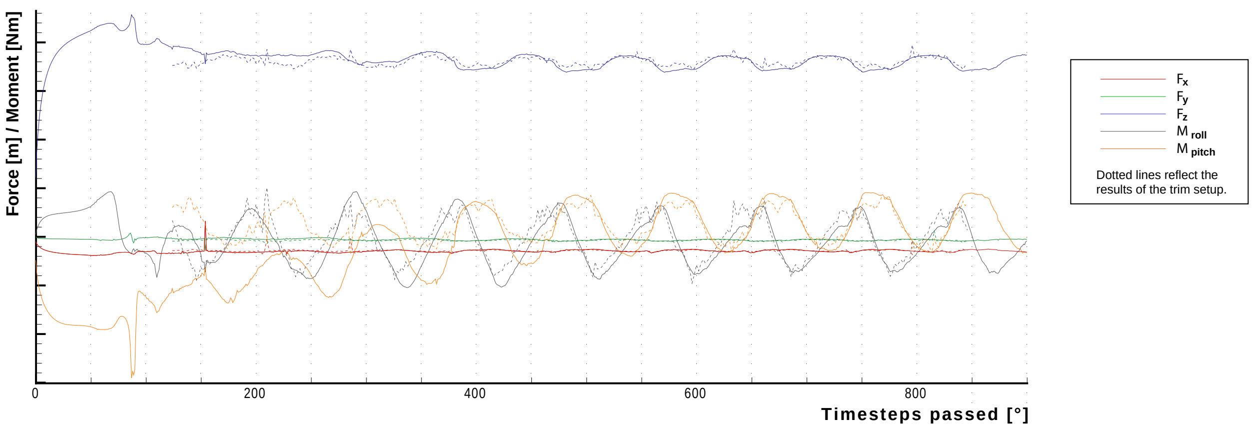

Figure 4. Force and moment progression over time for the complete main rotor. Solid lines illustrate the development after the restart of the refined setup. The dotted lines reflect the values at the end of the trim runs.

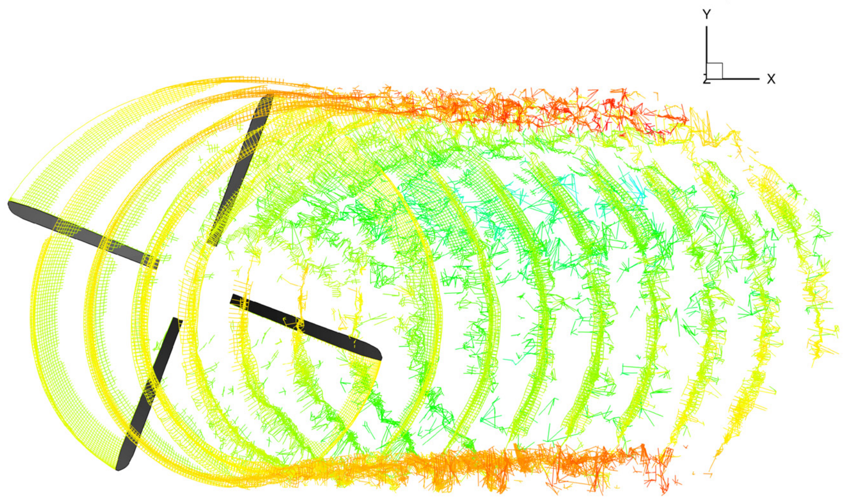

(a) Vortex layer visualization of the trim setup.

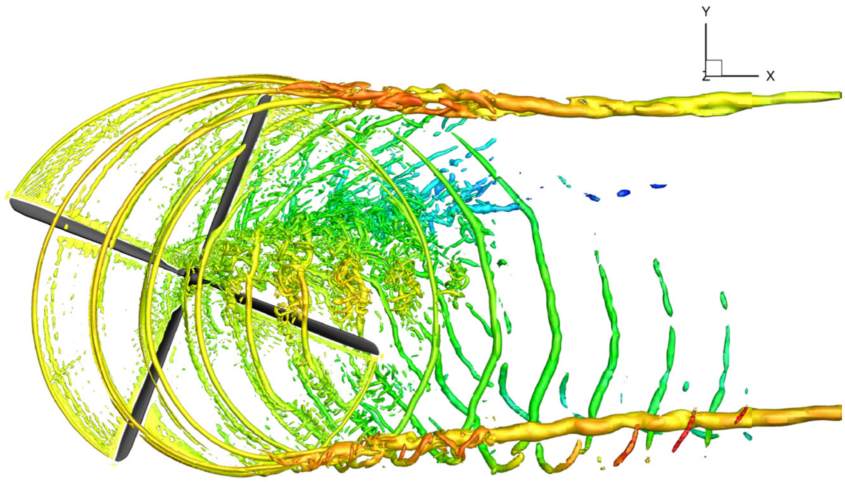

(b) CFD λ_2-visualization[1].

Figure 5. Qualitative comparison of the free wake to the CFD solution.

6 AERODYNAMIC VALIDATION AND ACOUSTIC ANALYSIS

For detailed investigation of the resulting flow field and for aeroacoustic analysis the temporal discretization of the free wake model is increased to a time step equivalent of 1 ° to achieve an acoustic resolution of 22.5 BPF. The number of trailers per rotor blade was doubled (to 50) to accomplish a smoother vorticity layer. To get a better understanding of convergence achieved, the refined setup is restarted from scratch using the deformation information resulting after the eighth retrim. As can be seen in Figure 4, complete convergence is achieved after 2.5 revolutions, respectively 900 time steps. The resulting global main rotor forces and moments match the values of the trim setup (dotted lines) almost exactly. Retrimming with the refined solution leads to changes of the trim angles of less than 0.05 °. This slight deviation lies within the accuracy of the tool chain, which validates the usage of a coarser setup for trimming purposes.

The detailed validation is separated into two thematical parts: The comparison of the aerodynamic flow field with a higher order CFD simulation, and the validation of the resulting aeroacoustic emissions, for which flight test data is available.

6.1 Aerodynamic validation

Figure 5 shows the resulting vortex filaments of the wake in comparison with a λ_2-plot of the CFD-reference solution. In both simulations the wake is dominated by the rotorblades' strong, compact tip vortices, which roll up to two longitudinal main wake vortices starting at $\psi = 90\,°$ and $\psi = 270\,°$. Both the shape and the location of the blade tip vortices within the rotor disc area are correct. By refining the setup, the average trailer distance is reduced to about 45 mm, whereby the vortex core radius of originally 25 mm is enlarged to 100 mm. The roll up of the wake in combination with the 1 °-timestep leads to vortex filament lengths of about 100 mm.

As a consequence, underdiscretization of the vorticity layer is still persisting, which becomes apparent by means of the chaotic arrangement of the vortex filaments within the major vortex structures. As the rotor head is not modelled, the highly turbulent flow behind, characterized by high density of small vortex structures, is not reflected by the free wake solution.

In Figure 6 the location of the vortex structures at an azimuth position of 75 ° is shown. It can be seen that the second and third BVI events at the advancing side are caused by the rollup of the vorticity layer of the own wake and of the wake of the directly subsequent blade, and not by the blade tip vortices themselves. Only the first BVI event is caused by the blade tip vortex of the preceding blade generated the revolution before. These findings and also the exact locations of the vortices match the results of the CFD reference solution by Kowarsch et al.[1].

The sectional lift distributions over one rotor revolution of the CFD and the free wake solution are oposed to each other in Figure 7. Slight differences can be seen for azimuth angles between $\psi = 90\,°$ and $\psi = 150\,°$ for relative rotor radii between $\frac{r}{R} = 0.70$ and $\frac{r}{R} = 0.85$. In this area, the rolling up vorticity layer is generated, which causes the second and third BVI events on the advancing side. The deviation is mainly caused by the simplified local pitching moments during the trim of the rotor, which leads to a slight underestimation of the geometric angle of attack, which corresponds again to an underestimation of the sectional lift. All other attributes of the lift distribution are qualitatively and quantitatively correctly reflected.

The investigated descent flight state is mainly characterized by the vertical inflow component. Due to the loss of height, relating to the helicopter's body frame, the inflow is pointing upwards, which leads to a reduction of the power required and consequently to a reduction of the induced velocity. The reduced downwash velocity in combination with upwards pointing inflow cause the blade tip vortices to cross the rotor disc vertically during their convection downstream, what leads to strong interaction phenomena with the subsequent rotor blades, called BVI. In Figure 7 the occurence of BVI and the accompanying local fluctuations of the sectional lift can be seen in both the free wake and the CFD solution as yellow shades in the azimuth ar-

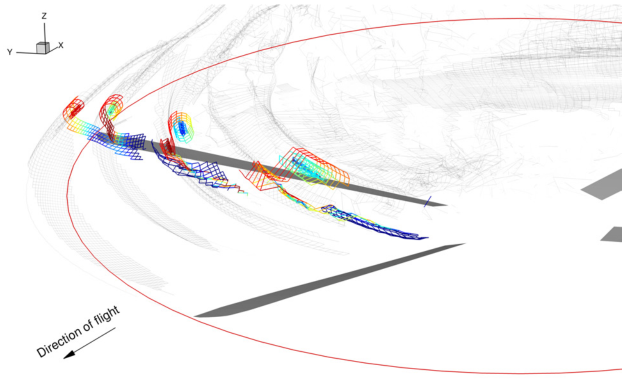

Figure 6. Location of the BVI generating vortex structures for $\psi = 75\,°$.

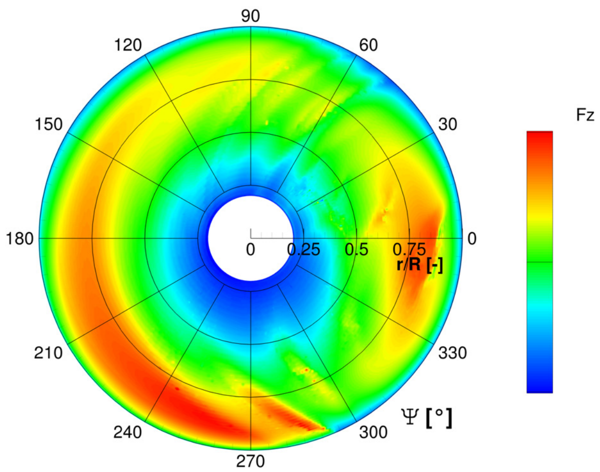

(a) Free wake

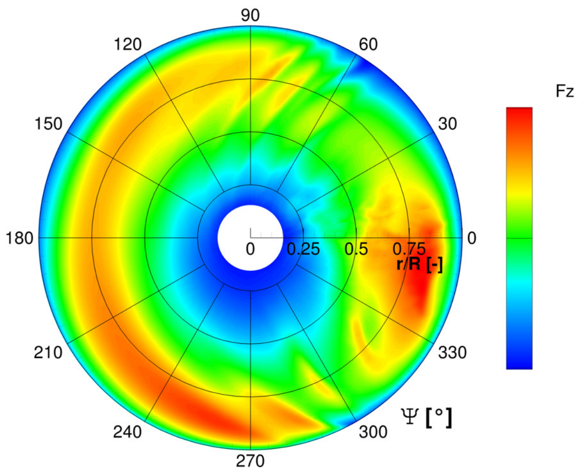

(b) CFD[1]

Figure 7. Sectional lift coefficient of the free wake solution in comparison to the CFD solution.

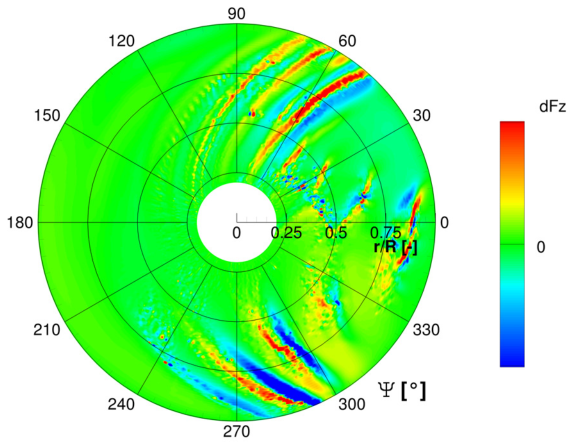

(a) Free wake (b) CFD[1]

Figure 8. Azimuthal (time) derivative of the sectional lift coefficient of the free wake solution in comparison to the CFD solution.

eas between $\psi = 50\,°$ and $\psi = 90\,°$, and $\psi = 260\,°$ and $\psi = 320\,°$.

For the investigated flight state, especially the BVI events are of high interest as they are one of the main drivers of the aeracoustic noise emission. The azimuthal derivative of the sectional lift (shown in Figure 8) gives a good first impression of the strength of the BVI events and their expected corresponding noise emissions. Both at the advancing and at the retreating blade side the sectional lift gradients of the CFD and the free wake solution are in good agreement. The number of BVI events, and position of occurence are correctly reproduced by the free wake solution. The deviation of the sectional lift within the second quadrant, as mentioned before, causes a slight undererstimation of the strength of the second and third BVI events at the advancing side. The first event at the advancing side and all events at the retreating side are captured correctly in terms of their strength.

By comparison with the coarser discretized trim setup, very limited differences for characteristics of the sectional lift can be seen: All BVI events are already catched (cf. Figure 9), but, due to the very limited temporal resolution of just 11.25 BPF, running an aeroacoustic analysis on the basis of this setup would disregard a large share of the BVI spectrum. Furthermore, the sectional lift gradients at the advancing blade are severely underpredicted, which would lead to a significant undererstimation of the resulting BVI noise.

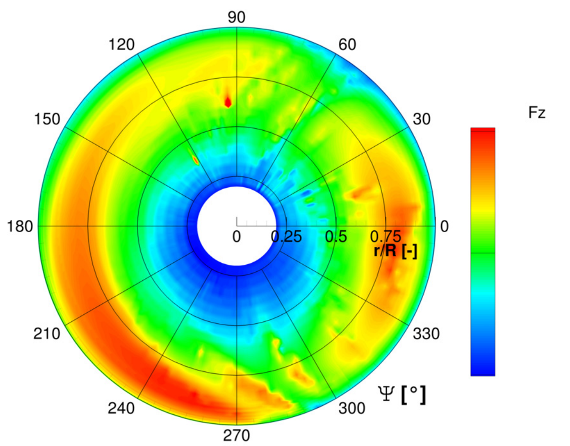

(a) Sectional lift coefficient (b) Azimuthal (time) derivative of the sectional lift coefficient

Figure 9. The trim setup's sectional lift and its azimuthal derivative.

6.2 Aeroacoustic validation

As a side effect of underdiscretizing the rotor blade's wake, very strong non-physical spikes result in the surface pressure and consequently in the sectionally integrated forces (cf. 10(a)). They occur when a vortex filament with strong vorticity passes a collocation point of the surface very closely. As a consequence of running the acoustic tool chain on this *spiky* aerodynamic solution, the computed noise emissions are dominated by the spikes and thus significantly overestimated. To overcome this problem, the spikes need to be filtered out without losing physically correct information, especially concerning the load gradients. As the spikes occur stochastically, this cannot be achieved within the frequency domain. Instead, the spikes are filtered out by averaging the sectional lift of multiple rotor revolutions for each datapoint followed by eliminating all datapoints, whose actual sectional lift value is exceeding the averaged lift by 20%. For the result shown in Figure 10(b) two complete revolutions were taken into account, what consequently leads for a four blade rotor to eight available values per data point.

The simulated fly-by maneuver takes about 40 s. To save time and computational ressources, and because of the periodic behaviour of undisturbed rotor flows, the aerodynamic solution is repeated multiple times by ACCO, while it is being shifted in space accordingly to the flight trajectory. Applying this procedure, numerically caused non-periodicities of the flow field lead to acoustic artefacts, which could ruin the aeroacoustic solution. To overcome this issue after eliminating the corrupt data, the remaining datapoints are *re*-averaged to force a periodic flow field as basis for the aeroacoustic computation.

A first qualitative comparison of the free wake solution to the CFD solution is performed on the basis of the noise footprint (cf. Figure 11). Therefore, a stationary noise carpet is computed by placing a dense mesh of observers moving with the helicopter's body frame 10 m below the rotor disk. The noise footprint shows a highly asymetric signature with a strong focus on the advancing side in upstream direction. This is expected in typical BVI flight situations. In comparison to the CFD solution, two out of three local maxima of the SPL distribution (marked with black borders) are met concerning their location, while the one located on the rear advancing side is underestimated. Quantitatively, the occuring maximum SPL values show a good agreement.

To get a quantitative impression of the results, the solution is compared with the flight test data of GP microphones published by Kowarsch et al.[1]. Since the experimental data contains the complete helicopter's noise, the main rotor noise was being extracted by selecting the tonal content of the main rotor (MR) from the total signal using blade passing frequency filtering. Figure 12 illustrates the microphone's Perceived Noise Level time-histories of the total and the filtered MR signal in comparison to the free wake and CFD results. The numerical data has been corrected by adding +6 dB to reflect the total reflection seen by the GP microphones.

In comparison to the flight test data, the gradient of the free wake solution while approaching the microphone array is predicted quite well. However, the past gradient is underpredicted and reaches for the retreating side and the center microphones values similar to the CFD solution. The decreasing gradient at the advancing side is also smaller in comparison to the CFD solution. This leads to diverging noise levels starting five to six seconds past the flyover. At the center and the advancing side microphone, the maximum values of the PNLT signal are correctly captured, whereas

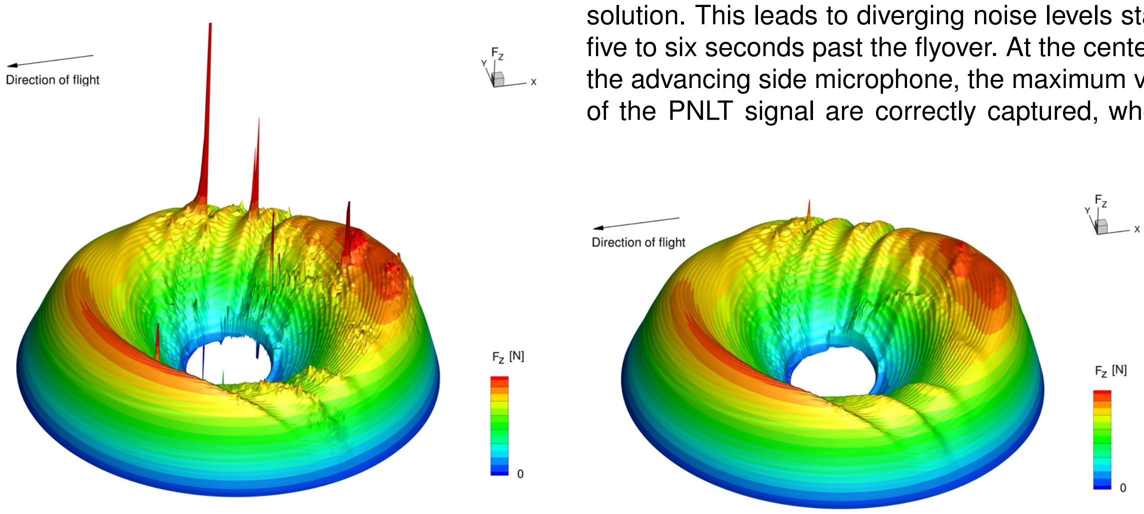

(a) Initial solution

(b) Averaged and filtered solution

Figure 10. Initial and filtered sectional integrated pressures on the blade surface over a complete revolution.

the maximum PNLT levels at the retreating side are slightly underestimated by ca. 2.5 dB. The trends are captured within acceptable tolerances. Especially the center and the retreating side microphones show a good agreement with the flight test data concerning their trend.

The certification relevant computation of the EPNL values start at the maximum PNLT values followed by the determination of the 10 dB down times t_1 and t_2. Within this time span the PNLT value is piecewise integrated. So for accurate EPNL predition a temporal and quantitative match of the maximum PNLT level and of the -10 dB transits is essential. For certification purposes within BVI flight situations mainly the center microphone signal is of relevance, as it dominates the noise emissions. The signal levels of the advancing side microphone and of the retreating side microphone are more than a magnitude smaller. As for the center microphone the maximum value and the -10 dB transits show a very good agreement to the experimental values, good prediction of the EPNL value

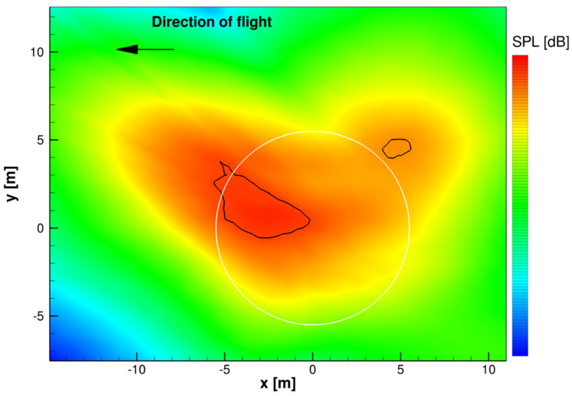

(a) Free wake

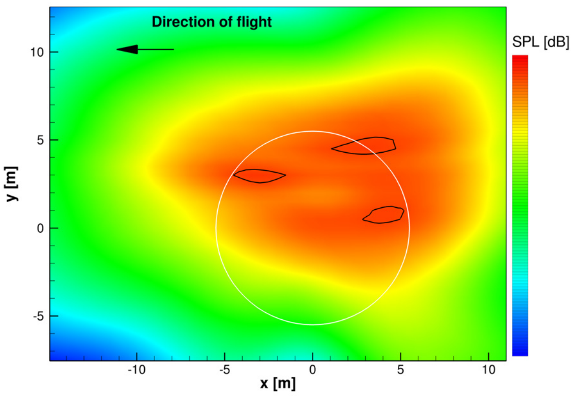

(b) CFD[1]

Figure 11. Moving noise carpet 10 m **below the rotor.**
(The rotor disk area is marked with a white circle. The local maxima are bordered in black.)

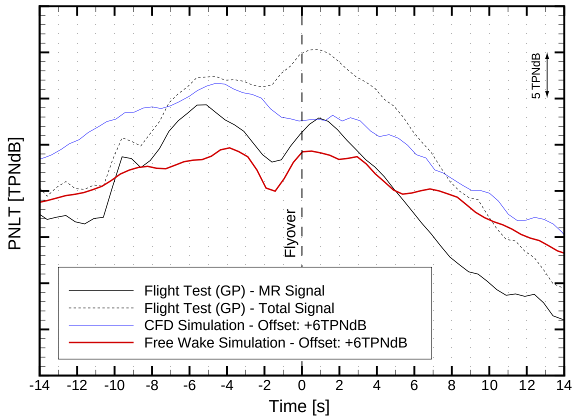

(a) Retreating side[1]

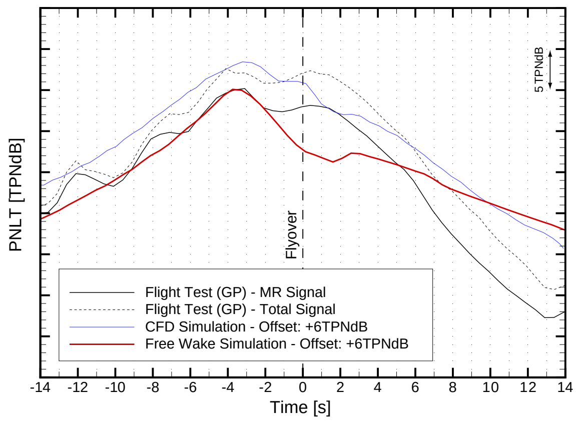

(b) Center[1]

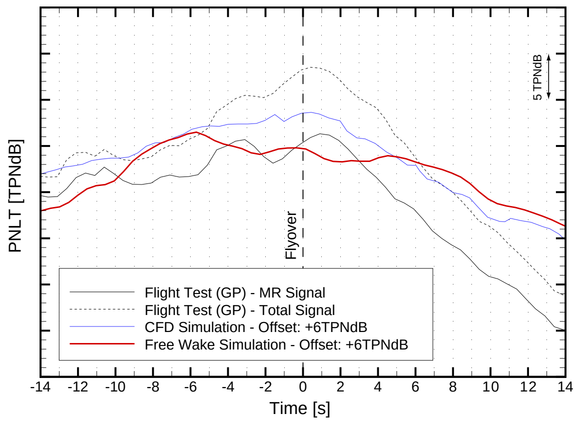

(c) Advancing side[1]

Figure 12. PNLT time history of flight test microphones.

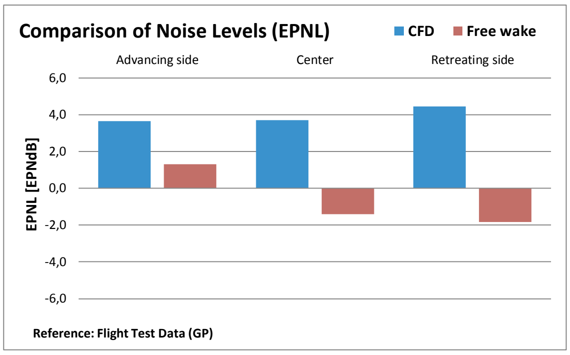

Figure 13. Comparison of EPNL noise levels.[1]

is expected, although its PNLT value falls below the experimental data for five seconds during the flyover.

As Kowarsch et al. mentioned, the extraction of the complete tonal content of the main rotor is difficult. Additionally, for the numerical solution reflection and shadowing is not taken into account. This might explain the slight underestimation of the advancing and retreating side microphones, which are within an acceptable range.

Figure 13 compares the resulting EPNL values with the experimental data and the CFD results. The EPNL values are quite well predicted for all three microphones (within ± 1.8 EPNdB). The highest deviation occurs at the retreating side with -1.8 EPNdB whereas the value at the advancing side, where BVI noise is dominating, is slightly overpredicted.

Although the exact trends of the PNL time histories are not perfectly reflected and requires further investigation, the current development state of the toolchain is able to predict EPNL values accurately–nearly within the tolerances defined by the certification regulations for experimental values. This enables the usage of the tool chain for industrial design processes of rotor systems.

7 CONCLUSIONS

The newly developed free wake method FIRST has been validated comparing aerodynamic results of a BVI descent flight state with CFD results, where the main rotor trim angles, the load distribution on the rotor disk, and its azimuthal gradient show good agreement. FIRST showed excellent robustness when varying both the spatial and temporal discretization and empirical parameters as the vortex core size. The free wake based tool chain is able to predict BVI noise emissions very accurately: the maximum deviaton of the EPNL values to the experimental data is only 1.8 dB. The EPNL values are slightly underpredicted in comparison to the main rotor noise extracted from flight test data. In comparison, the variation of flight test data allowed within the certification process is ± 1.5 dB.

As the most critical part the modelling of the lift generating structures was identified. A coarsely discretized lifting surface fails at predicting the correct pitching moments. Lifting lines are not able to catch three dimensional flow by design. Consequently, future work will focus on the validation of the implemented lifting body model with regard to its capabilities of predicting of the sectional pitching moment.

To quantify the influence of the discretization or empirical parameters as the vortex core size, a parameter study has been conducted, which will be published in the near future. Although the vortex core radius has no influence on the stability of the solution and on the resulting loads, within the parameter study the vortex core radius was identified as a main influence factor for the resulting aeracoustic values. Reducing vortex core size to values smaller than the averaged trailer distance causes an underestimation of the noise levels. This leads to a stochastic movement of the edge points of the vortex filaments within the major vortex structures. In consequence, not all of the originally chordwise directed vortex filaments being responsible for the BVI phenomenon are striking the rotor blade with the same angle at the same time, which reduces their influence on the loads occurring locally. On this account, the aeroacoustic evaluation shows lower EPNL values. The same applies to a spatial discretization chosen too coarsely. Besides its influence on the aeroacoustic frequency spectrum, the temporal discretization shows no significant influence on the solution. Summing up, FIRST behaves as expected on parameter variations and variations of the simulated flight situations.

The accurate prediction of noise emissions in combination with its robustness and performance makes FIRST a trustable and powerful tool within industrial rotor design processes.

Acknowledgments

Special thanks go to Ulrich Kowarsch for supplying the CFD-reference solution and for providing the acoustic post processing environment.

This work was performed within the federal research project ECO-HC2, which is lead by Airbus Helicopter Deutschland GmbH.

The authors would like to thank Airbus Helicopters Deutschland GmbH for the esteemed cooperation within this project and beyond, as well as providing us with experimental data to enable this investigation. We would like to express our thanks to the Federal Ministry of Economics and Technology for providing us with the resources to realize this project.

Further acknowledgement is made to the High Performance Computing Center in Stuttgart who provided us with support and service to perform the computations on their high performance computing system Hazel Hen.

Copyright Statement

REFERENCES

[1] Kowarsch, U., Lippert, D., Schneider, S., Keßler, M., and Krämer, E., "Aeroacoustic Simulation of an EC145T2 Rotor in descent flight", 71th American Helicopter Society Annual Forum, Virginia Beach, VA, 2015.

[2] Kowarsch, U., Öhrle, C., Keßler, M., and Krämer, E., "Aeroacoustic Simulation of a complete EC145T2 Helicopter in descent flight", 41th European Rotorcraft Forum, Munich, Germany, 2015.

[3] Zerle, L., *Aerodynamische und aeroakustische Rotorberechnung unter Anwendung frei entwickelter Nachlaufwirbelschichten und retardierter Potentiale*, Ph.D. thesis, Institut für Aerodynamik und Gasdynamik, Universität Stuttgart, 2000.

[4] Rankine, W., *A Manual of Applied Mechanics*, Charles Griffin and Company, 1872.

[5] Kaufmann, W., "Über die Ausbreitung kreiszylindrischer Wirbel in zähen Flüssigkeiten", *Ingenieur-Archiv*, Vol. 13, (1), 1962.

[6] Scully, M. P. and Sullivan, J. P., "Helicopter Rotor Wake Geometry and Airloads and Development of Laser Doppler Velocimeter for Use in Helicopter Rotor Wakes", Technical Report DSR No. 73032, Massachusetts Institute of Technology Aerophysics Laboratory, Cambridge, MA, 1972.

[7] Vatistas, G., Kozel, V., and Mih, W., "A simpler model for concentrated vortices", *Experiments in Fluids*, Vol. 1, (11), 1991, pp. 73–76.

[8] Schuff, M., Kranzinger, P. P., Keßler, M., and Krämer, E., "Advanced CFD-CSD Coupling: Generalized, High Performant, Radial Basis Function Based Volume Mesh Deformation Algorithm for Structured, Unstructured and Overlapping Meshes", 40th European Rotorcraft Forum, Southampton, UK, 2014.

[9] Kranzinger, P., Kowarsch, U., Schuff, M., Keßler, M., and Krämer, E., "Advances in Parallelization and High-fidelity Simulation of Helicopter Phenomena", *High Performance Computing in Science and Engineering 15*, edited by W. E. Nagel, D. H. Kröner, and M. M. Resch, Springer International Publishing, 2015, pp. 479–494.

[10] Johnson, W., *CAMRAD II Comprehensive analytical model of rotorcraft aerodynamics and dynamics*, fourth edition, 2009.

[11] Benoit, B., Kampa, K., von Grunhagen, W., Basset, P.-M., and Gimonet, B., "HOST, a General Helicopter Simulation Tool for Germany and France", *Proceedings of the 56th Annual Forum of the American Helicopter Society*, Vol. 56, (2), 2000, pp. 1110–1131.

[12] Dietz, M., Schimke, D., and Embacher, M., "Advanced Industrial Application of CFD for Helicopter Development", Proceedings of the 36th European Rotorcraft Forum, Paris, France, September 2010.

[13] Keßler, M. and Wagner, S., "Source-Time Dominant Aeroacoustics", *Computers & Fluids*, Vol. 33, 2004, pp. 791–800.

[14] International Civil Aviation Organization, Environmental, *Technical Manual - Volume I: Procedures for the Noise Certification of Aircraft*, doc. 9501 edition, 2012.

[15] Gareton, V., Gerais, M., and Heger, R., "Acoustic Design and Testing of the Eurocopter EC145T2 and EC175B - a harmonized Franco-German Approach", 39th European Rotorcraft Forum, Moscow, 2013.

[16] Young, L., "Vortex Core Size in the Rotor Near-Wake", Technical Report NASA/TM-2003-212275, A-03010293, NASA Ames Research Center; Moffett Field, CA, 2003.